Si powders and electrodes for high-energy lithium-ion cells

Richard T. Haasch, [a] Stephen E. Trask, [b] Marco-T. F. Rodrigues, [b] and Daniel P. Abraham [b]

[a] *Materials Research Laboratory, University of Illinois at Urbana-Champaign, Urbana, Illinois, 61801, USA*

[b] *Chemical Sciences and Engineering Division, Argonne National Laboratory, Lemont, Illinois, 60439, USA*

Rechargeable lithium-ion batteries (LIBs) are electrochemical energy-storage devices that are used in diverse applications ranging from small-sized consumer electronic devices, mid-sized electric vehicles, to the large-scale electricity grid. In their basic form, a LIB cell contains two electrodes at which redox reactions occur during electrochemical cycling, an electrolyte that transports lithium-ions between the electrodes, and a separator that prevents the electrodes from contact with each other while allowing the movement of ions.

Commercial lithium-ion batteries (LIBs) typically contain graphite as the electrochemically active material in the negative electrode. The graphite could be partially or fully replaced by silicon in next-generation, high energy density, LIBs because the theoretical lithium storage capacity of silicon is about ten times greater than that of graphite. However, the commercialization of silicon-based electrodes has been hindered by the large volume changes (up to 320%) that result from the insertion/extraction of lithium-ions into/from silicon particles; graphite, in comparison, displays a ~10% volume change. Additionally, the electrochemical alloying/dealloying with lithium fractures the silicon particles and increases their surface area, which in turn increases parasitic side-reactions that trap lithium-ions and degrades battery performance.

Various strategies are pursued to improve the performance and longevity of silicon-containing LIBs. Modifying the silicon particle surfaces to minimize reactivity with the electrolyte and maximize interactions with the polymer binder ranks high among these approaches. Utilizing coatings to enhance the electronic contact within the electrode matrix is especially important for silicon, given that these particles have an oxide surface layer that forms during material synthesis. Additionally, surface modification can also prevent H_2 evolution reactions that occur during water-based electrode fabrication processes, which consume active material and, at large enough scales, can pose safety hazards (Ref. 1).

In this study, we report X-ray photoelectron spectroscopy data from various surface-modified silicon powders (Table I) obtained from a commercial vendor (Paraclete Energy, Inc.). The powders were produced by milling and contain Si particles with a mean diameter of ~150 nm. Data are presented from Si particles coated with a thin carbonaceous layer (Si/C, Ref. 2), and

from Si/C particles with additional coatings based on polyethylene glycol (PEG) (Ref. 3), polyvinylene difluoride (PVdF) (Ref. 4), and perfluorooctene (PFO) (Ref. 5). Data from particles covered with only the native oxide layer (n-SiO, Ref. 6) are also reported here. Spectra from Si-based composite *electrodes* (Table II) based on the powders described above and containing carbon (for electronic conduction), graphite (for limiting the overall electrode expansion) and partially-lithiated polyacrylic acid (Li-PAA, for binding) are also included (Refs. 7-12). The Li-PAA was prepared by titrating polyacrylic acid (PAA) with 1 M LiOH in an aqueous solution; exchanging the protons with Li^+ ions reduces coiling of the PAA polymer chains and improves their adhesion to the particles (Ref. 13).

XPS measurements of the powder and anode samples were made using a Kratos Axis Ultra X-ray photoelectron spectrometer (Kratos Analytical, Inc., Manchester, UK) using monochromatic Al K_α radiation (1486.6 eV). High-resolution spectra were collected from a single spot at an emission angle of 0˚ at a pass energy of 40 eV from a 0.7 mm x 0.3 area using the hybrid (electrostatic and magnetic immersion) lens mode. The samples were affixed onto the conductive sample holder with insulating double-sided transparent tape. The sample holder was then loaded onto the grounded sample stage. The binding energy scale of the instrument was calibrated using the Cu 2p (932.6 eV) and Au 4f (84.0 eV) photoelectron lines. The binding energies were referenced to the bulk Si 2p signal at 99.3 eV. The pressure during analysis was *ca.* 7×10^{-7} Pa.

Description of XPS data and Highlights

XPS data collected from the raw powders are shown in Figs. 1-4. As these materials are surface-modified silicon particles it was anticipated that there may be differences in the chemical/electronic nature of the surface of the particles between the various materials. Therefore, the bulk Si 2p signal is used as an energy reference instead of the more typical -CC-, -CH signal. The spectra show products of oxidation of the particle surfaces, which occur during synthesis, as well as the carbon coatings formed during the surface modification process.

A comparison of the C 1s spectra collected from the powder materials are shown in Fig. 1. Overall, the spectra of the raw powders have fairly similar peak shapes. All materials show intensities at ~285.1 [-CC-, -CH], ~286.7 [-C-O], and ~289.3 [O-C=O] eV. Intensities at ~283.3 [SiC_x, $(1 < x < 2)$] are also observed for all powders, except n-SiO. The fluorine-containing Si/C/PVdF and Si/C/PFO-based particles show additional intensity for the C 1s spectra at ~286.7 [-C-O], ~289.1 [O-C=O], 291.6 [-$\underline{C}F_2CF_3$] and ~294.0 [-$CF_2\underline{C}F_3$] eV. The absence of intensity at 290.0 eV [-($\underline{C}F_2CH_2)_n$-] in the Si/C/PVdF-based particles suggests that the PVdF has decomposed during the particle modification process. The expectation of a variation of the chemical/electronic nature of the surfaces of these materials is confirmed by evidence of small differences in the position of the -CC-, -CH signal.

The Si 2p regions from the powder materials are compared in Fig. 2. The Si/C, Si/C/PEG, and n-SiO powders show intensities at ~99.3 [Si], ~100.5 [SiO_y, (1 < y < 2)], ~102.6 [SiC_xO_y], and ~103.3 eV [SiO_2,] eV. The fluorine-containing Si/C/PFO powder shows additional intensity in the Si 2p spectra at 102.8 eV [SiF_z (1 < z < 4) (Ref. 15)].

The O 1s spectra collected from the powder materials, shown in Fig. 3, indicate intensities at ~532.2 [-C=O, O-C=O, SiO_y] and ~533.5 [-C-O] eV. As the PEG and PFO-based powders are the only ones with a carbon/oxygen containing additive, it is presumed that the additional oxygen signal in the C 1s spectra is due to oxidation that occurred during the particle synthesis process.

A comparison of the F 1s spectra from the raw Si/C/PVdF and Si/C/PFO powders is shown in Fig. 4. Signals were observed at ~686.7 [SiF_z (Ref. 15), SiO_aF_b], and ~688.7 [CF_2CF_3] eV. Si/C/PFO powder shows a signal at 685.2 [NaF] possibly due to processing of the powder. The presence of signal due to SiF_z in both the Si 2p and F 1s spectra from the Si/C/PFO-based powders suggests a Si-PFO side reaction occurred during the modification process.

Figures 5-8 show XPS data collected from electrodes made using the surface-modified silicon particles described above. These spectra show not only the constituent elements of the surface-modified silicon particles, but also the other components used to fabricate the electrodes. A comparison of the C 1s spectra collected from the electrodes are shown in Fig. 5. The C 1s spectra of electrodes fabricated with the Si/C, and Si/C/PEG materials show signals at ~282.8 [SiC_x, (1 < x < 2)], ~283.9 [graphite, carbon black], ~285.3 [-CC-, -CH], ~287.2 [-C-O], and 289.2 [O-C=O] eV. Electrodes fabricated using Si/C/PVdF and Si/C/PFO particles show contributions at ~289.0 [O-C=O] and 293.9 [$-CF_2\underline{C}F_3$] eV.

The Si 2p regions collected from electrodes fabricated with the surface-modified silicon particles are shown in Fig. 6. As signal from silicon comes only from the surface-modified particles, the spectra appear to be fairly similar to those of the raw powders. The Si/C, Si/C/PEG, and n-SiO materials show intensities at ~99.3 [Si], ~100.5 [SiO_y, (1 < y < 2)], ~102.3 [SiC_xO_y], and ~103.4 eV [SiO_2]. The fluorine-containing Si/C/PVdF and Si/C/PFO-based electrodes shows additional intensity in the spectra at 102.3 eV [SiC_xO_y, SiF_z (1 < z < 4) (Ref. 15)] and 103.3 eV [SiO_2, SiO_aF_b].

The O 1s spectra collected from the electrodes fabricated with the surface-modified silicon particles are shown in Fig. 7. These spectra also appear to be fairly similar to those of the raw particles. The spectra indicate intensities at ~532.3 [-C=O, O-C=O, SiO_y] and ~533.6 [-C-O] eV. The F 1s spectra from the electrodes are shown in Fig. 8. Both the Si/C/PVdF-based Si/C/PFO-based electrodes indicates signals at ~685.6 [LiF] and ~686.7 [SiO_aF_b] The Si/C/PFO-based electrode shows additional signal 688.8 [CF_2, CF_3] eV.

Surface quantification of the raw silicon-modified particles and the electrodes is summarized in Table III. In general, the elemental composition trends are as expected. The high C content

observed on the n-SiO powder suggests that the silicon is covered by a carbonaceous compound that is likely a residue of the milling process used to produce the particles.

Summary of Electrochemistry data

Stainless steel based 2032-type coin cells were used for the electrochemical tests. The cells contained the electrodes shown in Table II along with a Li-metal counter electrode, Celgard 2325 separator and an electrolyte with 10 wt% FEC added to a solution of 1.2M $LiPF_6$ in EC:EMC (3:7, w/w); $LiPF_6$ is lithium hexafluorophosphate, EC is ethylene carbonate, EMC is ethyl methyl carbonate and FEC is fluoroethyl carbonate. The electrochemical tests were conducted at 30 °C using a MACCOR Series 4000 test unit; the cells were cycled in the 1.0-0.1 V range at a ~C/25 rate.

The first cycle lithiation and delithiation capacities, and coulombic efficiencies, are given in Table IV; the associated cycling plots are given in Fig. 9. The specific capacities are based on the weight of all electrochemically active materials (silicon, graphite, carbon black) in the electrode. As expected, the 15Si/C cell has the lowest capacity (and the highest coulombic efficiency) as the electrode has the lowest silicon content. The 90Si/C composition has the lowest coulombic efficiency possibly due to silicon particle disconnection from the electron conduction network after the initial lithiation; unlike the others, this electrode does not contain carbon black, which enables electron percolation through the matrix. All cells containing the 70Si/C material displayed good performance; the PVdF modified sample has a lower delithiation capacity than the non-coated electrode, whereas the PFO and PEG modified samples display improved performance. We postulate that these capacity differences arise from dissimilarities in the composition of the solid electrolyte interphases (SEIs) formed during the electrochemical cycle. Fig. 10 shows the differential capacity (dQ/dV) peak associated with electrolyte reduction during the first cycle and SEI formation; peaks are present for all samples, except 90Si/C. In all cases, the peak is centered in the 1.0 – 1.1 V range, which is characteristic of FEC reduction. The small variations in peak location and intensity suggests subtle differences in electrolyte reduction (and possibly SEI composition) for the various samples. The apparent lack of a ~1.0 V peak for the 90Si/C sample maybe from the increased polarization (and hence delayed solvent reduction) resulting from the absence of carbon black in the electrode.

Acknowledgments

This work was carried out in part in the Materials Research Laboratory Central Research Facilities, University of Illinois. The authors acknowledge support from the Office of Vehicle Technologies at the U.S. Department of Energy. The electrodes examined in these studies were fabricated at Argonne's Cell Analysis, Modeling and Prototyping (CAMP) Facility, which is supported within the core funding of the Applied Battery Research (ABR) for Transportation Program. We are grateful to Jeff Norris of Paraclete Energy for providing the silicon materials. The submitted manuscript

References

1. M. -T. F. Rodrigues, S. E. Trask, I. A. Shkrob, D. P. Abraham, "Quantifying gas generation from slurries used in fabrication of Si-containing electrodes for lithium-ion cells", *J. Power Sources* **395**, 289 (2018).
2. R. T. Haasch, D. P. Abraham, "Si-based materials for lithium-ion batteries I. Si/C powder," *Surf. Sci. Spectra*, Submitted.
3. R. T. Haasch, D. P. Abraham, "Si-based materials for lithium-ion batteries II. Si/C/polyethylene glycol powder," *Surf. Sci. Spectra*, Submitted.
4. R. T. Haasch, D. P. Abraham, "Si-based materials for lithium-ion batteries III. Si/C/polyvinylidine fluoride powder," *Surf. Sci. Spectra*, Submitted.
5. R. T. Haasch, D. P. Abraham, "Si-based materials for lithium-ion batteries IV. Si/C/perfluorooctene powder," *Surf. Sci. Spectra*, Submitted.
6. R. T. Haasch, D. P. Abraham, "Si-based materials for lithium-ion batteries V. n-SiO powder," *Surf. Sci. Spectra*, Submitted.
7. R. T. Haasch, D. P. Abraham, "Si-based materials for lithium-ion batteries VI. 15% Si/C-graphite/carbon black/lithiated polyacrylic acid electrode," *Surf. Sci. Spectra*, Submitted.
8. R. T. Haasch, D. P. Abraham, "Si-based materials for lithium-ion batteries VII. 70% Si/C-carbon black/lithiated polyacrylic acid electrode," *Surf. Sci. Spectra*, Submitted.
9. R. T. Haasch, D. P. Abraham, "Si-based materials for lithium-ion batteries VIII. 90% Si/C–lithiated polyacrylic acid electrode," *Surf. Sci. Spectra*, Submitted.
10. R. T. Haasch, D. P. Abraham, "Si-based materials for lithium-ion batteries IX. 70% Si/C/polyethylene glycol–carbon black/lithiated polyacrylic acid electrode," *Surf. Sci. Spectra*, Submitted.
11. R. T. Haasch, D. P. Abraham, "Si-based materials for lithium-ion batteries X. 70% Si/C/polyvinylidine fluoride–carbon black/lithiated polyacrylic acid electrode," *Surf. Sci. Spectra*, Submitted.
12. R. T. Haasch, D. P. Abraham, "Si-based materials for lithium-ion batteries XI. 70% Si/C/perfluorooctene–carbon black/lithiated polyacrylic acid electrode," *Surf. Sci. Spectra*, Submitted.
13. Z. –J. Han, K. Yamagiwa, N. Yabuuchi, J.-Y. Son, Y.-T. Cui, H. Oji, A. Kogure, T. Harada, S. Ishikawa, Y. Aokid, S. Komaba, "Electrochemical lithiation performance and characterization of silicon–graphite composites with lithium, sodium, potassium, and ammonium polyacrylate binders" *Phys.Chem.Chem.Phys.* ***17****, 3783 (2015).*
14. G. Beamson and D. Briggs, High Resolution XPS of Organic Polymers, The Scienta ESCA300 Database (John Wiley & Sons, Chichester, 1992), pp 236-7.
15. T. J. Chuang, *Journal of Applied Physics* **51**, 2614 (1980).

TABLE I. Si powders. C, F, O and Si spectra were obtained from these powder materials

Powder	Description
Si/C	Si coated with 2.5 wt% carbon
Si/C/PEG	Si coated with 2.5 wt% carbon, further modified with 4 wt% PEG
Si/C/PVdF	Si coated with 2.5 wt% carbon, further modified with 4 wt% PVdF
Si/C/PFO	Si coated with 2.5 wt% carbon, further modified with 4 wt% PFO
n-SiO	Si with native oxide layer

TABLE II. Anodes with Si (see Table I), Graphite (Gr), carbon black (CB) and LiPAA

Electrode	Si type, wt%	Gr, wt%	CB, wt%	LiPAA, wt%
15Si/C	Si/C, 15%	73	2	10
70Si/C	Si/C, 70%	…	15	15
90Si/C	Si/C, 90%	…	…	10
70Si/C/PEG	Si/C/PEG, 70%	…	15	15
70Si/C/PVdF	Si/C/PVdF, 70%	…	15	15
70Si/C/PFO	Si/C/PFO, 70%	…	15	15

TABLE III. Surface compositions of the powder and anode samples measured by XPS

Sample	F, at%	O, at%	C, at%	Si, at%
Si/C	…	21.7	42.0	36.3
Si/C/PEG	…	17.2	66.7	16.1
Si/C/PVdF	3.8	17.1	51.0	28.1
Si/C/PFO	15.3	14.2	44.3	26.1
n-SiO	…	21.6	51.2	27.2
15% Si/C	…	21.3	68.9	9.9
70% Si/C	…	25.7	52.3	22.0
90% Si/C	…	29.7	34.6	35.7
70% Si/C/PEG	…	27.0	45.5	27.5
70% Si/C/PVdF	4.0	28.4	43.2	24.5
70% Si/C/PFO	12.1	23.1	43.0	21.8

TABLE IV. First cycle capacities and coulombic efficiencies of electrodes with Si

Electrode	Si type, wt%	Lithiation, mAh/g	Delithiation, mAh/g	Coulombic Efficiency, %
15Si/C	Si/C, 15%	527	460	87.3
70Si/C	Si/C, 70%	1606	1375	85.7
90Si/C	Si/C, 90%	1823	962	52.8
70Si/C/PVdF	Si/C/PVdF, 70%	1554	1264	81.3
70Si/C/PFO	Si/C/PFO, 70%	2218	1904	85.8
70Si/C/PEG	Si/C/PEG, 70%	2098	1721	82.1

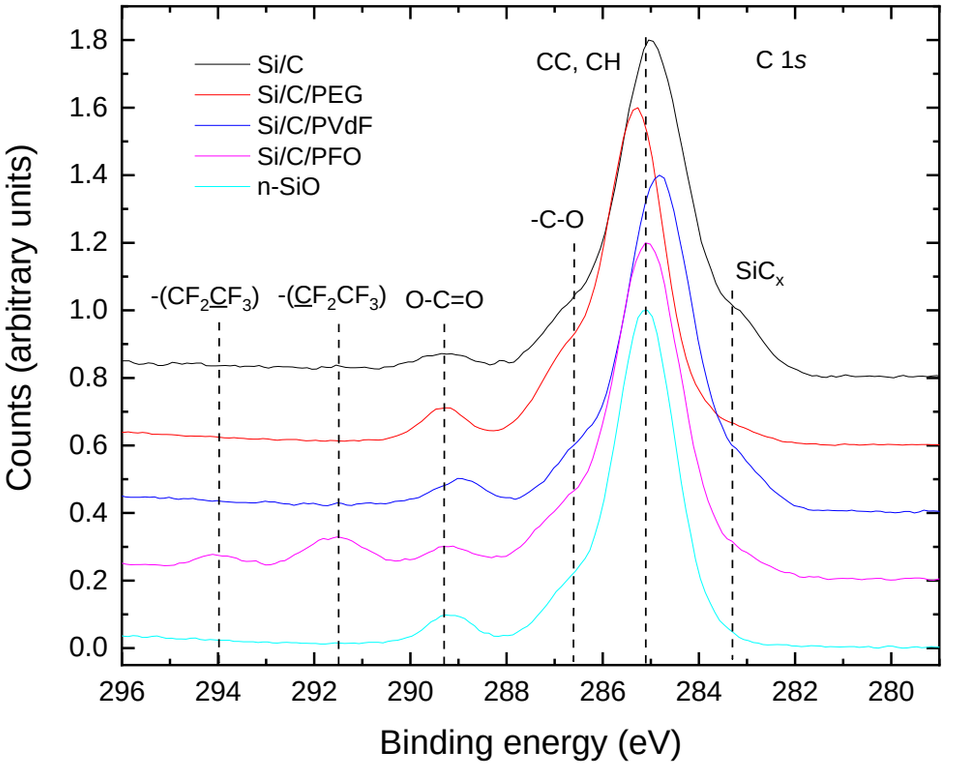

Fig. 1. C 1s spectral comparison of the silicon-based Si/C, Si/C/PEG, Si/C/PVdF, Si/C/PFO, and n-SiO powders.

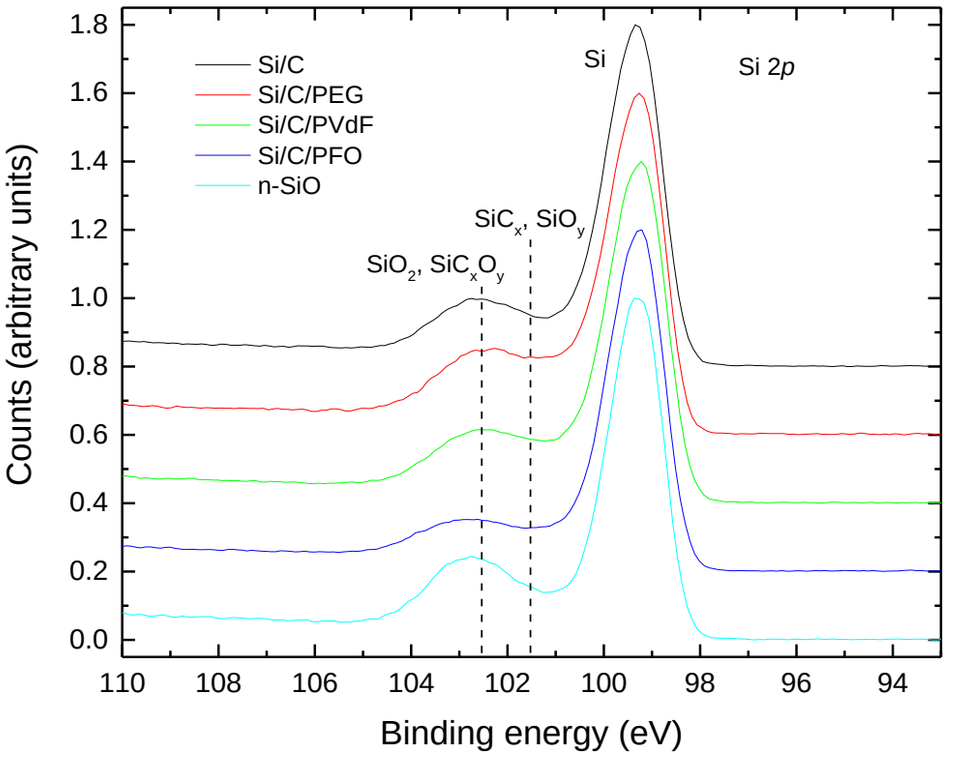

Fig. 2. Si 2p spectral comparison of the silicon-based Si/C, Si/C/PEG, Si/C/PVdF, Si/C/PFO, and n-SiO powders.

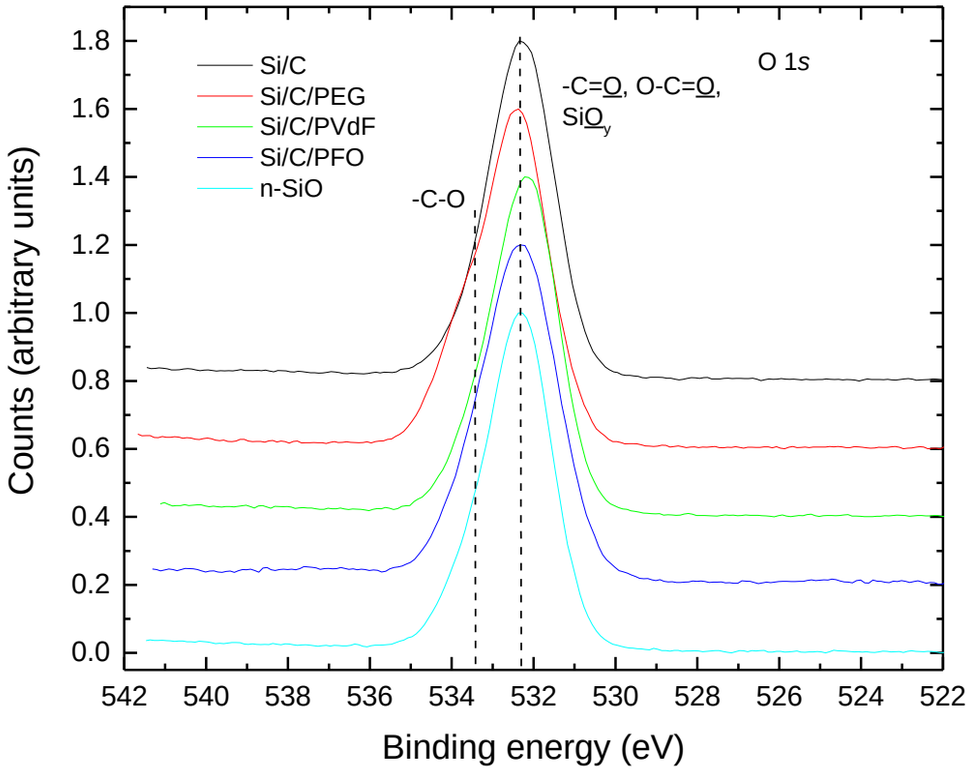

Fig. 3. O 1s spectral comparison of the silicon-based Si/C, Si/C/PEG, Si/C/PVdF, Si/C/PFO, and n-SiO powders.

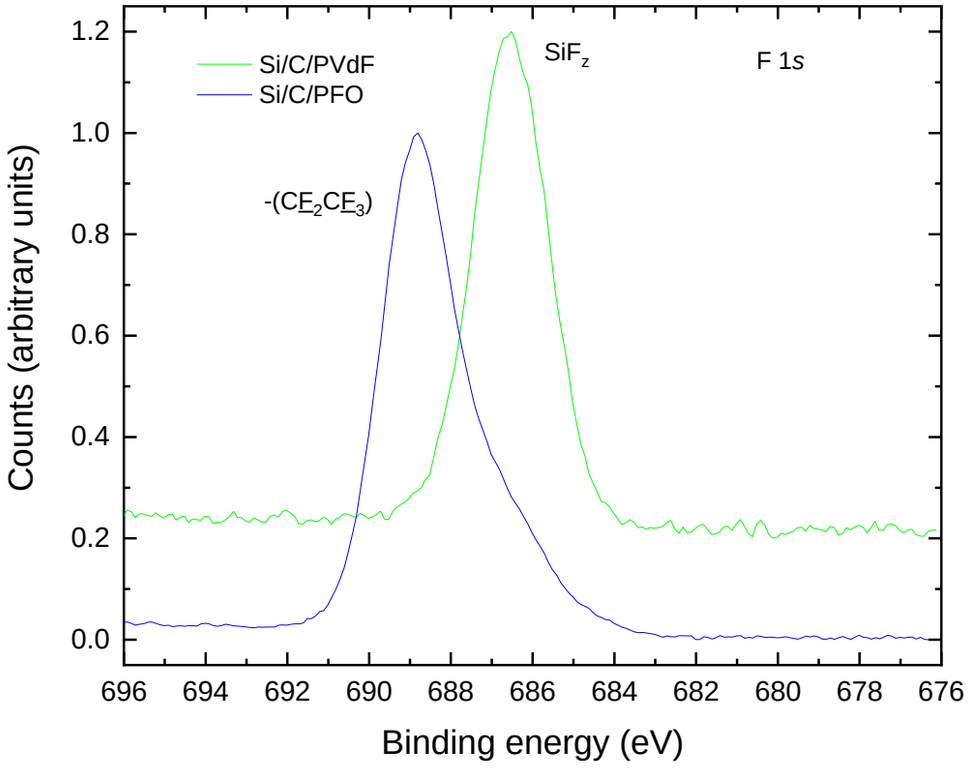

Fig. 4. F 1s spectral comparison of the silicon-based Si/C/PVdF and Si/C/PFO powders.

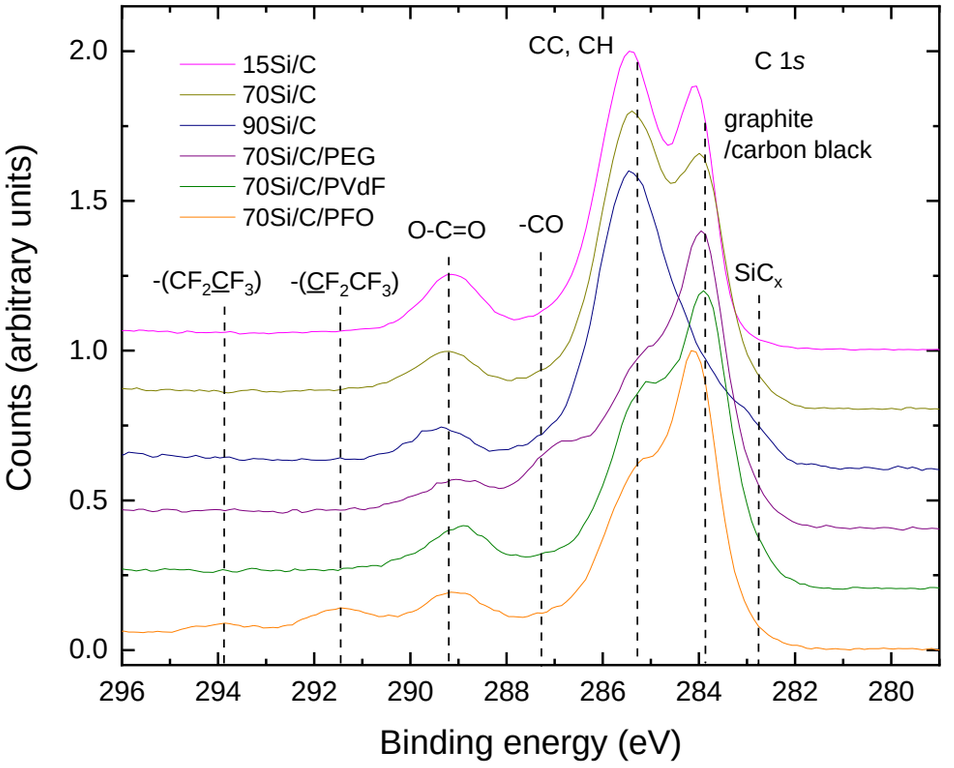

Fig. 5. C 1s spectral comparison of the 15Si/C, 70Si/C, 90Si/C, 70Si/C/PEG, 70Si/C/PVdF, and 70Si/C/PFO-based electrodes.

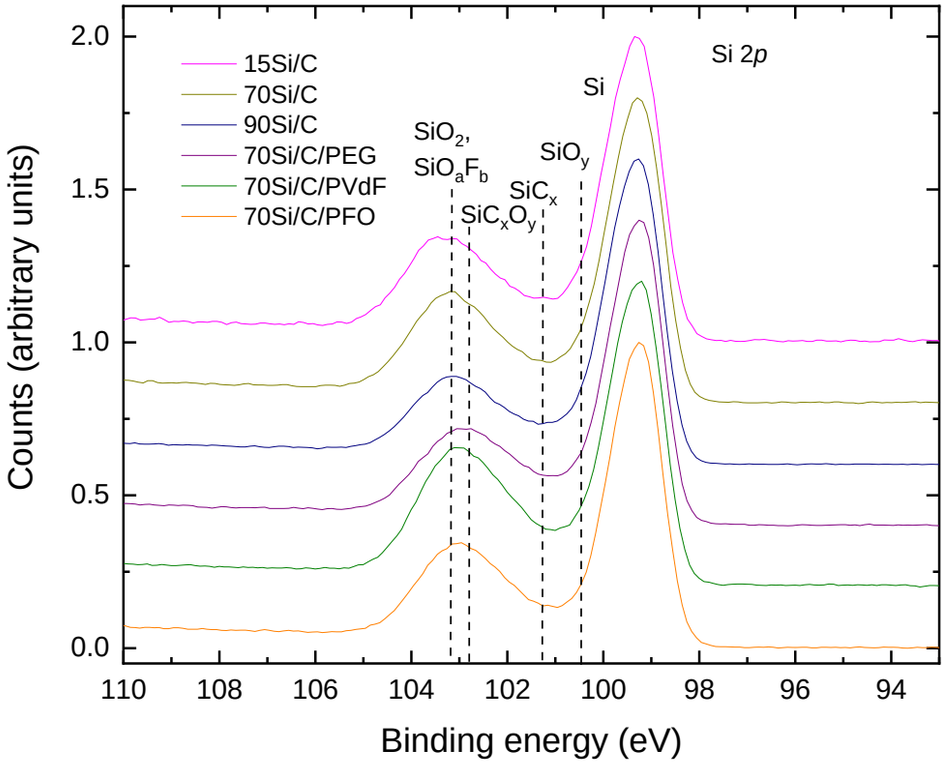

Fig. 6. Si 2p spectral comparison of the 15Si/C, 70Si/C, 90Si/C, 70Si/C/PEG, 70Si/C/PVdF, and 70Si/C/PFO-based electrodes.

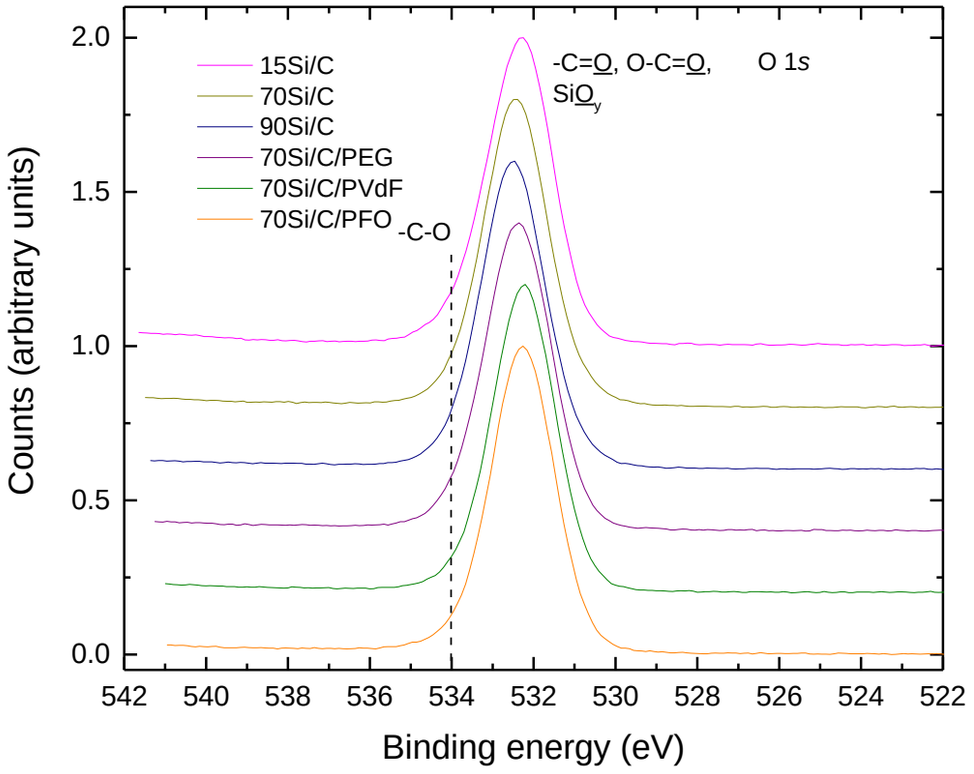

Fig. 7. O 1s spectral comparison of the 15Si/C, 70Si/C, 90Si/C, 70Si/C/PEG, 70Si/C/PVdF, and 70Si/C/PFO-based electrodes.

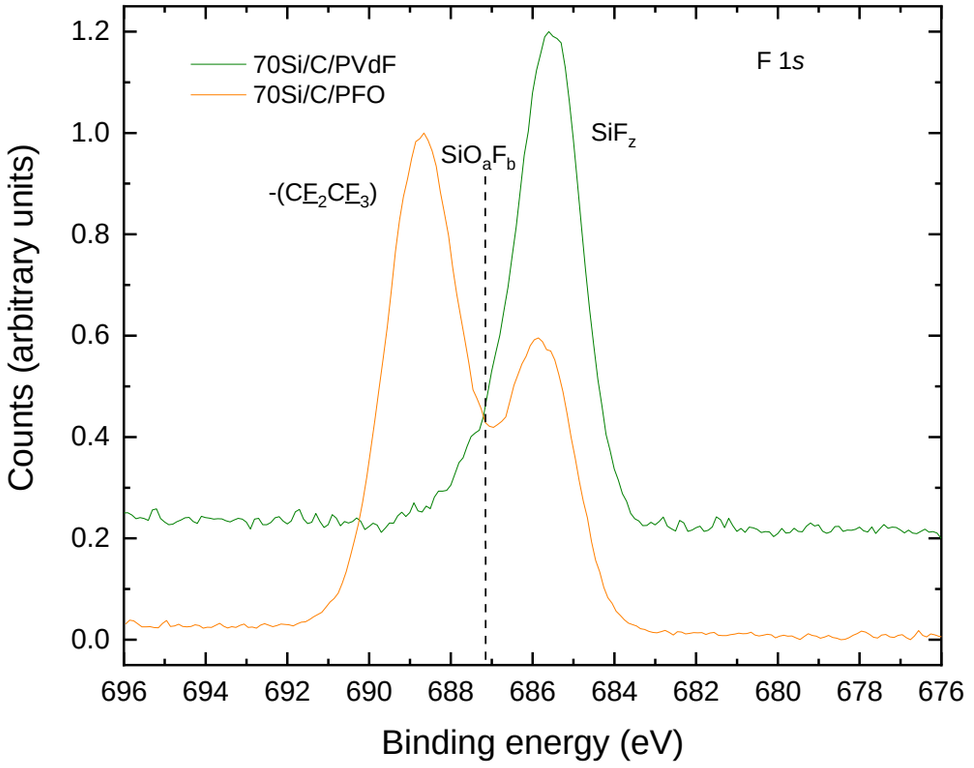

Fig. 8. F 1s spectral comparison of the 70Si/C/PVdF and 70Si/C/PFO-based electrodes.

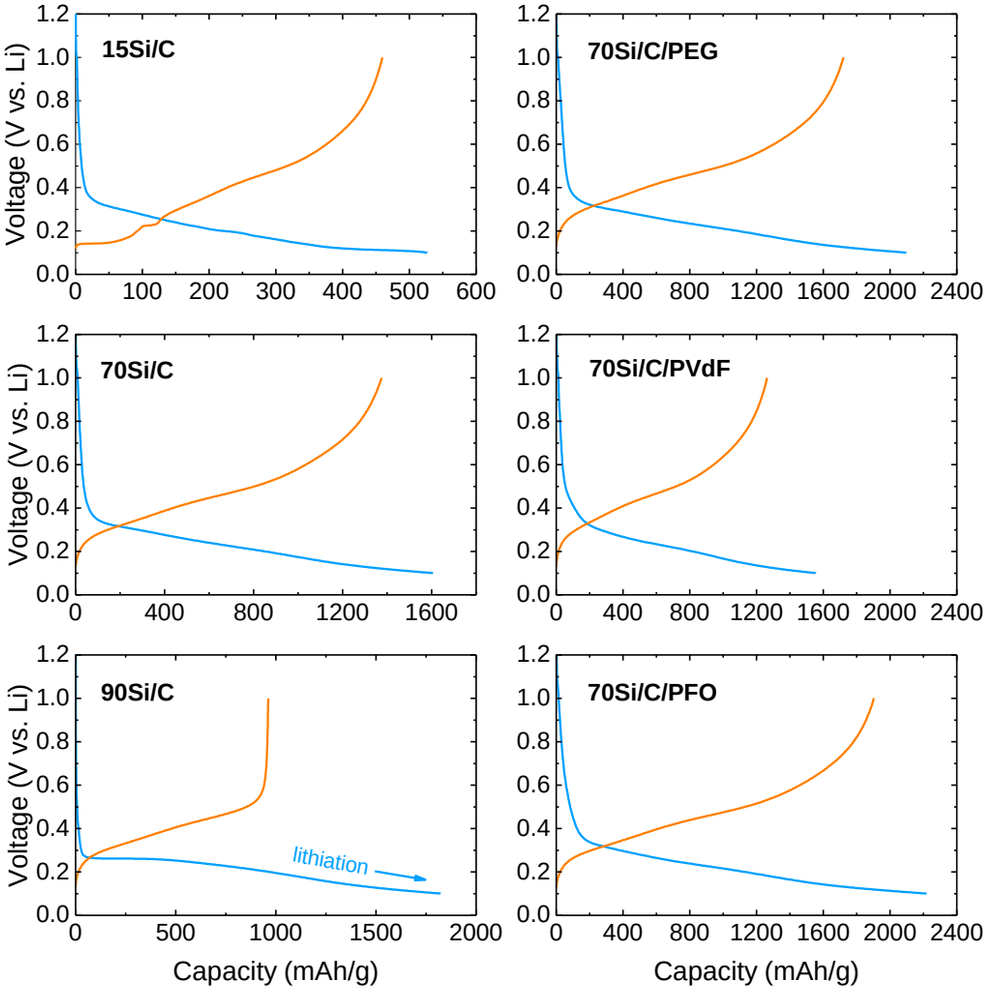

Fig. 9. Electrode potential changes during the first lithiation/delithiation of half-cells (i.e. *versus* a Li counter electrode) with the 15Si/C, 70Si/C, 90Si/C, 70Si/C/PEG, 70Si/C/PVdF, and 70Si/C/PFO electrodes. The cells were cycled in the 1.0 – 0.1 V range at ~C/25 rate and 30 °C. The specific capacity was calculated using the weight of all active components (silicon, carbon black, graphite) in the electrode.

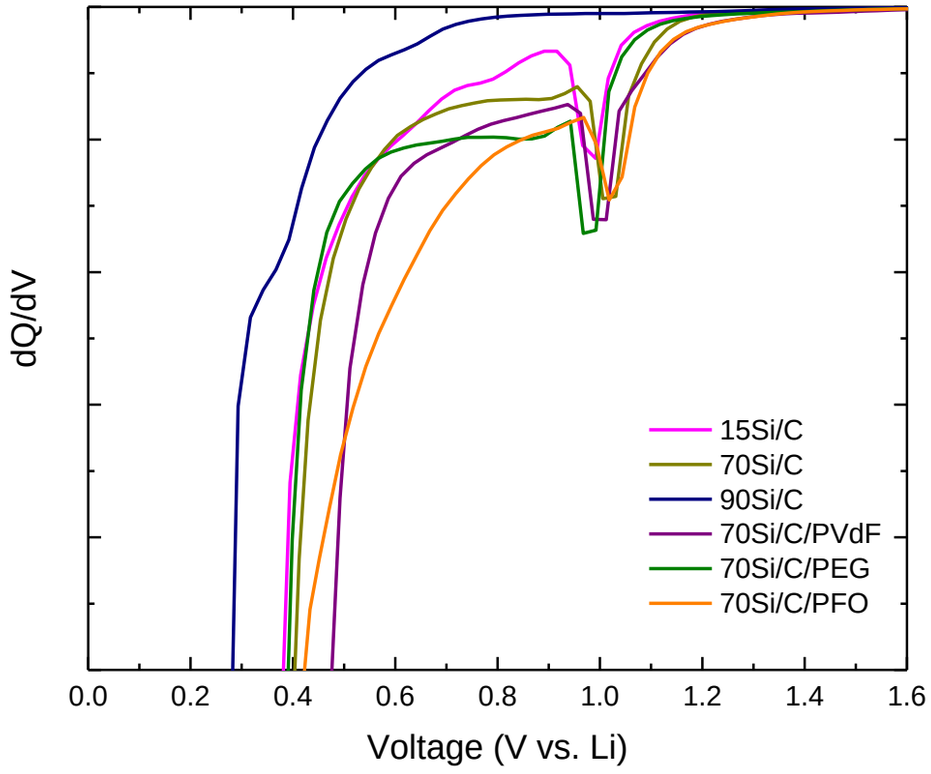

Fig. 10. Differential capacity (dQ/dV) as a function of voltage during the first lithiation of half-cells (i.e. Li counter electrode) with the 15Si/C, 70Si/C, 90Si/C, 70Si/C/PEG, 70Si/C/PVdF, and 70Si/C/PFO electrodes. The peak observed at ~1.0 – 1.1 V is not observed during subsequent lithiation cycles.